

# 1 **A new fluorescence-based approach for direct visualization of coat formation during** 2 **sporulation in *Bacillus cereus***

3  
4 Armand Lablaine<sup>a&</sup>, Stéphanie Chamot<sup>a</sup>, Mónica Serrano<sup>b</sup>, Cyrille Billaudeau<sup>c</sup>, Isabelle Bornard<sup>d</sup>, Rut  
5 Carballido-Lopez<sup>c</sup>, Frédéric Carlin<sup>a</sup>, Adriano O. Henriques<sup>b</sup> and Véronique Broussolle<sup>a\*</sup>

6  
7 <sup>a</sup>INRAE, Avignon Université, UMR SQPOV, F-84000 Avignon, France

8 <sup>b</sup>Instituto de Tecnologia Química e Biológica, Universidade Nova de Lisboa, 2780-157 Oeiras, Portugal

9 <sup>c</sup>MICALIS Institute, INRAE, AgroParisTech, Université Paris-Saclay, 78350 Jouy en Josas, France

10 <sup>d</sup>INRAE, Pathologie végétale, F-84143 Montfavet, France

11 <sup>&</sup> present address: MICALIS Institute, INRAE, AgroParisTech, Université Paris-Saclay, 78350 Jouy en Josas,  
12 France

13 \* address correspondence: veronique.broussolle@inrae.fr

14

15

## 16 **Abstract**

17 The pathogenic bacteria *Bacillus cereus*, *Bacillus anthracis* and *Bacillus thuringiensis* form spores encased in  
18 a protein coat surrounded by a balloon-like exosporium. These structures mediate spore interactions with its  
19 environment, including the host immune system, control the transit of molecules that trigger germination  
20 and thus are essential for the spore life cycle. Formation of the coat and exosporium has been traditionally  
21 visualized by transmission electronic microscopy on fixed cells. Recently, we showed that assembly of the  
22 exosporium can be directly observed in live *B. cereus* cells by super resolution-structured illumination  
23 microscopy (SR-SIM) using the membrane MitoTrackerGreen (MTG) dye. Here, we demonstrate that the  
24 different steps of coat formation can also be visualized by SR-SIM using MTG and SNAP-cell TMR-star dyes  
25 during *B. cereus* sporulation. We used these markers to characterize a subpopulation of engulfment-defective  
26 *B. cereus* cells that develops at a suboptimal sporulation temperature. Importantly, we predicted and  
27 confirmed that synthesis and accumulation of coat material, as well as synthesis of the  $\sigma^K$ -dependent protein  
28 BxpB, occur in cells arrested during engulfment. These results suggest that, unlike the well-studied model  
29 organism *Bacillus subtilis*, the activity of  $\sigma^K$  is not strictly linked to the state of forespore development in *B.*  
30 *cereus*.

31

32

33

34

35

## 36 Introduction

37 Sporulation is a developmental process in which a vegetative cell transforms into a highly resilient  
38 spore (Fig. 1). Among the spore forming bacteria, endospores (hereinafter simply referred to as 'spores')  
39 made by *Firmicutes* species, which include the model organism for developmental studies *Bacillus subtilis*,  
40 the foodborne pathogen *B. cereus*, its closely relatives *B. anthracis* and *B. thuringiensis*, and the nosocomial  
41 pathogen *Clostridioides difficile*, are of particular interest for developmental biology or clinical studies<sup>1,2</sup>.

42 Transmission electronic microscopy (TEM) has traditionally been the technique used to study the  
43 formation and architecture of *Firmicutes* spores<sup>3</sup>. Pioneer TEM studies revealed that the general architecture  
44 of spores and the sporulation steps are conserved among *Firmicutes* species<sup>4</sup>. Firstly, the cell entering  
45 sporulation divides asymmetrically into a small cell, the forespore and a larger mother cell, both defining a  
46 sporangium (Fig. 1). Then, the mother cell membrane migrates around the forespore in a phagocytosis-like  
47 process so-called engulfment. Ultimately, the mother cell lyses releasing a mature spore in the environment  
48 (Fig. 1). The mature spore consists in a series of concentric shells, with from the center to the outside, the  
49 dehydrated core containing the genetic information, the primordial germ cell wall, the cortex, a layer of  
50 modified peptidoglycan, which is wrapped in a complex proteinaceous external shell. The architecture of the  
51 proteinaceous surface shell differs greatly between bacterial species<sup>2,5,6</sup>, likely reflecting the niches in which  
52 spores persist and eventually germinate, ranging from the soil, the oxygen-deprived mammalian gut, or the  
53 inhospitable macrophages<sup>2,7</sup>. Hence, while the spores of *B. subtilis* are encased in a multilayered thick  
54 proteinaceous coat, the spores of species belonging to the *B. cereus* group are enclosed in a thin layer of  
55 coat surrounded by a balloon-like exosporium, both structures being separated by an interspace presumably  
56 filled by polysaccharides (Fig. 1)<sup>8</sup>.

57 Compared to other *Firmicutes* spore-formers, and thanks to its high natural transformability, the  
58 assembly of the multilayered coat of *B. subtilis* has been studied in depth and is now well understood<sup>1,6,9,10</sup>.  
59 Notably, most of the known coat proteins of *B. subtilis* were localized during sporulation by conventional  
60 fluorescence microscopy, using GFP-fusions inserted at the original genetic locus and the model of *B. subtilis*  
61 coat assembly largely originates from those studies<sup>1,6,9</sup>. In contrast, for species of the *B. cereus* group, genetic  
62 manipulations remain limited by its low transformability<sup>11,12</sup> and GFP or mCherry fusions are, most of the  
63 time, carried on shuttle plasmids<sup>13-21</sup>. In addition, for *B. cereus sensu stricto* species, and in contrast to *B.*  
64 *anthracis*, GFP-fusions were ineffective to localize early or late assembling exosporium proteins<sup>13,22</sup>. Hence,  
65 the model of coat and exosporium assembly mainly originates from TEM analysis of fixed cells (Fig. 1)<sup>15,18,23-</sup>  
66 <sup>26</sup>. Coat assembly appears to differ greatly in *B. subtilis* and *B. cereus*, as the initiation of this assembly process  
67 occurs in opposite regions of the forespore<sup>15,18</sup>. Despite such a fundamental difference, formation of the *B.*  
68 *cereus* coat remains a poorly studied process and an alternative way allowing the direct observation of

69 proteinaceous layers formation in live cells would be of interest to better characterize this developmental  
70 process.

71 Although coat assembly begins early after formation of the mother cell among *Firmicutes* species,  
72 the coat is clearly visible by classical TEM only after engulfment completion and is not detected in  $\Delta sigK$   
73 sporangia<sup>5,15,18,23,24,27-29</sup>. In *B. subtilis*, activation of the late sporulation sigma factor  $\sigma^K$  is tightly coupled to  
74 engulfment completion through several levels of regulation, including delayed transcription of the *sigK* gene,  
75 removal of an inhibitory pro-sequence and excision of a prophage-like skin element from the  $\sigma^K$ -encoding  
76 gene<sup>29-33</sup>. Despite a high conservation of sigma factor primary sequence, difference in the control of SigK  
77 activation had been reported among *Firmicutes* species<sup>29</sup>. Notably, in *C. difficile*, an inhibitory  $\sigma^K$  pro-  
78 sequence is absent and  $\sigma^K$  activity occurs during engulfment as well as in engulfment-defective cells<sup>34-38</sup>. The  
79 activity of  $\sigma^K$  in engulfment-defective cells leads to the synthesis and the accumulation of electron-dense  
80 coat material at, or close to the forespore surface, observed by TEM and referred as a “coat bearding”  
81 phenotype<sup>35</sup>. For most *B. cereus* strains, a  $\sigma^K$  pro-sequence is present, while the *sigK* gene is not interrupted  
82 by a prophage sequence as in *B. subtilis* and *C. difficile*. Whether  $\sigma^K$  activation and accumulation of coat  
83 material is linked to engulfment completion in *B. cereus* is not known.

84 We recently showed that the exosporium layer could be visualized in *B. cereus* live sporulating cells  
85 and spores using the membrane dye Mitotracker green (MTG) and Structured Illumination Microscopy  
86 (SIM)<sup>15</sup>. Using MTG and a SNAP-fusion for the exosporium cap protein CotY, we showed the existence of a  
87 second small exosporium cap at the mother cell proximal pole (MCD pole) of  $\Delta exsY$  spores not previously  
88 observed by TEM<sup>25,26</sup>. This indicates that exosporium formation shares more similarities with the *B. subtilis*  
89 model of coat formation than expected<sup>1,2,39,40</sup>. Here, we show that SNAP-cell TMR-star (TMR-star), a  
90 fluorescent substrate used to label SNAP-tag fusion proteins, and MTG are both able to specifically bind to  
91 the coat surface of *B. cereus*. The resulting fluorescent signals observed in sporangia and in spores can be  
92 used to determine precisely the stage of coat assembly. Using SIM analysis, we observe fluorescence signals  
93 that we assigned to an accumulation of coat material in engulfment-defective *B. cereus* cells, which was  
94 confirmed by TEM analysis. Finally, we demonstrate that the SNAP-tag fusion allows to successfully detect  
95 the late assembling BxpB exosporium protein and that both the TMR-star association with the *B. cereus* coat  
96 and the TMR-star signal labeling the BxpB-SNAP fusion are detected in engulfment-defective *B. cereus* cells.  
97 Our results provide a new way to evaluate the state of surface layers formation in live sporangia and suggest  
98 that regulation of  $\sigma^K$  activation is weakly linked to the state of forespore development in the *B. cereus* group,  
99 indicating that pathogenic spore-formers deploy different strategies to control this step of spore formation.

100

101

## 102 Results

103 **TMR-star and MTG bind to the forespore surface and their signal localization reflects the pattern of**  
104 **coat deposition.** We previously used the self-labelling SNAP-tag to determine the localization of early  
105 assembling exosporium proteins during *B. cereus* sporulation<sup>15</sup>. Indeed, SNAP-protein fusions can be  
106 localized by fluorescence microscopy upon addition of a cell-permeable fluorescent ligand<sup>41</sup>. Surprisingly, we  
107 noticed that the TMR-star, a red fluorescent SNAP substrate, also labeled the surface of spores that do not  
108 harbor any SNAP-tag fusion (Fig. 2A, TMR channel in panel *h*)<sup>15</sup>. The coat of *Firmicutes* spores bind different  
109 fluorescent substrates<sup>37,42–46</sup> and in *B. cereus* ATCC 14579 wild-type cells (WT14579), the TMR-star signal  
110 displayed a particular ellipsoid shape (Fig. 2A, panel *h*, cyan arrows) inside the exosporium layer (Fig. 2A,  
111 panel *h*, pink arrow), matching the localization of the coat. We thus wondered whether binding of TMR-star  
112 to the spore surface of *B. cereus* could be used as a coat marker in fluorescence microscopy studies. Coat  
113 deposition in the *B. cereus* group is a sequential process (Fig. 1), with electron-dense coat material firstly  
114 appearing on the long side of the forespore<sup>15,18,23</sup>. In the absence of the exosporium cap, as in cap-defective  
115  $\Delta cotE$  cells, the sequence of coat deposition is altered and coat deposition can initiate on the forespore poles  
116 (Fig. 1)<sup>15,18</sup>. We reasoned that, if TMR-star binds to *B. cereus* coat, intermediate TMR-star signals should be  
117 observed during sporulation and would be impacted by the absence of the exosporium cap. Thus, we carefully  
118 examined the TMR-star signal during the sporulation of WT14579 (Fig. 2A) and of a congenic  $\Delta cotE$  mutant  
119 (Fig. 2B). We induced sporulation by resuspension in SMB at 20°C, since  $\Delta cotE$  spores can be partly de-coated  
120 at this suboptimal temperature<sup>47</sup>. Sporulating cells and spores collected throughout sporulation were labeled  
121 with TMR-star and the MTG membrane dye and imaged with bright field (BF) and super-resolution SIM  
122 illumination modes.

123 In both WT14579 and  $\Delta cotE$  sporangia, the TMR-star signal appeared after engulfment and was first  
124 observed incompletely covering the surface of engulfed forespore (Fig. 2A and B, panels *e* and *f*, cyan arrows).  
125 Under BF illumination, the forespore of those sporangia appeared dark, indicating the development of  
126 forespore refringency (panels *e* and *f*, yellow asterisks). In WT14579 sporangia showing a TMR-star signal  
127 partially covering the forespore surface (in the MTG channel), the basal layer of the exosporium cap appeared  
128 clearly more extended from the forespore membrane (Fig. 2A, panels *e* and *f*,  $504 \pm 109$  nm,  $n=35$ ), than in  
129 WT14579 sporangia without TMR-star signal (panel *d*,  $219 \pm 73$  nm,  $n=48$ ). This result indicates that binding  
130 of TMR-star on the forespore surface is concomitant to exosporium extension. Visual inspection of SIM  
131 reconstructed images also revealed a brighter MTG signal partly covering the periphery of refringent  
132 forespores with a TMR-star signal (Fig. 2A and B, panels *e-f*). The pattern of MTG brighter signal localization  
133 differed between WT14579 and  $\Delta cotE$  sporangia (panels *e* and *f* in Fig. 2A and B) but remarkably, in both  
134 cases, this localization fully reflected the patterns of coat deposition previously described by TEM in *B. cereus*  
135 and in *B. anthracis* (Fig. 1)<sup>15,18,23</sup>. Finally, in  $50 \pm 7\%$  of  $\Delta cotE$  spores (144/263 cells from two independent

136 experiments), both the MTG and the TMR-star signals partially covered the spore surface (Fig. 1B, panel *h*,  
137 see Materials and methods), while a total coverage was observed in WT14579 spores (Fig. 1A, panel *h*). We  
138 concluded that the TMR-star and MTG bright signals observed in sporangia and in spores match all features  
139 of coat assembly previously described by TEM in both *B. cereus* and *B. anthracis*<sup>15,18,23,47</sup>.

140

#### 141 **Quantification of MTG signal intensity in sporangia.**

142 To determine if the brighter MTG signals observed on the periphery of refringent forespores reflect  
143 MTG binding to additional structures (other than the cell membrane), we quantified the ratio of the MTG  
144 signal intensity between the forespore and the mother cell (FS/MC MTG fluorescence intensity) in WT14579  
145 and  $\Delta cotE$  sporangia at different sporulation stages (Fig. 3A, see also red boxes in Fig. 2A and Material and  
146 Methods). Before engulfment completion, the forespore and the mother cell compartments are located side  
147 by side (Fig. 1), and we therefore expected a FS/MC MTG fluorescence intensity ratio of 1 (Fig. 3A, red dashed  
148 line) towards the MCD pole of the forespore (Fig. 1). Just after engulfment completion, the forespore is  
149 surrounded by two membranes, in close proximity (Fig. 1) and the theoretical FS/MC MTG fluorescence  
150 intensity ratio is then equal to 2. In line with these predictions, the average FS/MC MTG fluorescence intensity  
151 ratio was  $0.93 \pm 0.21$  (median  $\pm$  standard deviation,  $n=153$ ) and  $0.99 \pm 0.23$  ( $n=316$ ) in WT14579 and  $\Delta cotE$   
152 sporangia respectively, at an intermediate stage of engulfment (Fig. 3A, "engulfing", see red boxes in MTG  
153 channel of panel *a* of Fig. 2A). In sporangia with an engulfed forespore (red boxes in panel *d* of Fig. 2A), the  
154 FS/MC MTG fluorescence intensity ratio was  $1.78 \pm 0.28$  ( $n=211$ ) and  $1.81 \pm 0.29$  ( $n=143$ ) in WT14579 and  $\Delta cotE$ ,  
155 respectively (Fig. 3A). In sporangia with a TMR-star signal incompletely covering the surface of the refringent  
156 forespore ("incomplete", red boxes in panel *e* of Fig. 2A), the FS/MC MTG fluorescence intensity ratio locally  
157 increased to  $3.50 \pm 1.30$  ( $n=92$ ) and to  $6.05 \pm 1.91$  ( $n=131$ ) in WT14579 and  $\Delta cotE$  sporangia, respectively (Fig.  
158 3A). These observations suggest that, in addition to the two membranes that delineate the forespore contour,  
159 the MTG dye associates with an additional structure on the forespore surface, giving a brighter signal in  
160 sporangia of refringent forespores. Finally, the FS/MC MTG fluorescence intensity ratio decreased to  
161  $2.08 \pm 0.56$  ( $n=156$ ) when the TMR-star homogeneously covered the forespore surface of WT14579 sporangia  
162 ("complete", red boxes in panel *e* of Fig. 2A), only slightly higher than the ratio obtained in sporangia with no  
163 TMR-star signal on the surface of engulfed forespores ( $1.78 \pm 0.28$ ) (Fig. 3A). In contrast, the ratio of FS/MC  
164 MTG fluorescence intensity was similar in  $\Delta cotE$  sporangia of refringent forespores showing incomplete TMR-  
165 star labelling ( $6.05 \pm 1.91$ ) and in sporangia with a TMR-star fully covering the forespore surface ( $5.37 \pm 2.04$ ,  
166  $n=44$ ). Our quantification of the fluorescence signals suggests that, once fully assembled, the coat becomes  
167 less permeable to MTG in WT sporangia. However, this was not observed in  $\Delta cotE$  sporangia, suggesting that  
168 coat properties are altered, even if the coat seems fully assembled on the forespore surface.

169

170 **The coat is partly assembled in engulfment-defective *B. cereus* cells.** We previously reported that  
171 sporulation of *B. cereus* ATCC 10876 (WT10876) at 20°C leads to abnormal engulfment phenotypes in a  
172 variable proportion of the sporulating cells<sup>15</sup>. To determine whether formation of coat material depends on  
173 engulfment completion in *B. cereus*, we analyzed coat assembly in engulfment-defective WT10876 cells. We  
174 first confirmed, using a dual labeling of cell membranes with FM4-64 and MTG<sup>48,49</sup>, that engulfment was  
175 indeed aborted in a fraction of the WT10876 sporulating cells at 20°C (Supplementary Fig. S1A, cyan arrows).  
176 Additionally, using a forespore fluorescent reporter (*PspoIIQ*-YFP), we observed bulging of the forespore  
177 towards the mother cell cytosol (Supplementary Fig. S1B, cyan arrows), a phenotype associated with impaired  
178 septal degradation of peptidoglycan<sup>50-54</sup>. In agreement with these observations, SIM revealed that the  
179 developing forespore pushes across the asymmetric septum and forms a bulge into the mother cell cytoplasm  
180 at hour 24 (Fig. 4A panels *a-c*). At hour 48, sporangia with a bulging phenotype never became refringent (Fig.  
181 4A, panels *d-e* and Supplementary Fig. S1A, red asterisk), in contrast to sporangia with a normally engulfed  
182 forespore (Fig. 4A panel *g* and Supplementary Fig. S1A, yellow asterisks). Interestingly, TMR-star signals were  
183 detected in non-refringent-bulging sporangia (Fig. 4A, panels *d* and *e*, cyan arrows) and co-localized with  
184 bright MTG signals (curved and straight fragments; yellow and red arrows, respectively), suggesting the  
185 presence of coat material. Furthermore, the shape and the localization of TMR-star and MTG signals was  
186 strikingly similar to the particular mislocalization of coat fragments, also referred as “coat bearding”,  
187 previously observed in engulfment-defective *C. difficile* cells<sup>35</sup>. Finally, at hour 72, corresponding to the time  
188 of spore release (Fig. 4A, panel *f*, yellow asterisks), rare bulging sporangia were still present and we mainly  
189 detected abundant curved fragments (cyan arrows) sprinkled in the media, indicating that bulged sporangia  
190 ultimately lysed.

191 We performed a quantitative analysis of the FS/MC MTG fluorescence intensity ratio in WT10876  
192 engulfment-defective sporangia (Fig. 3A and B, see also Materials and methods), showing TMR-star/MTG  
193 bright signals (“bearding”) or not (“bulging”). We performed the quantification for both the MCD and the  
194 mother cell proximal pole regions (MCP, here the forespore bulge) as the FS/MC MTG fluorescence intensity  
195 ratio should differ in these two regions of a partially engulfed forespore (See light and dark blue boxes in Fig.  
196 3B). In the MCD region of bulging sporangia, the FS/MC MTG fluorescence intensity ratio was  $0.92 \pm 0.25$   
197 ( $n=77$ ) (Fig. 3A and B), confirming that only one membrane is present in this forespore region, while in the  
198 MCP region the ratio was  $1.80 \pm 0.37$  ( $n=77$ ) (Fig. 3A and B), as in engulfed WT14579 forespores with no TMR-  
199 star signal (Fig. 3A). In sporangia showing a bearding phenotype, the FS/MC MTG fluorescence intensity ratio  
200 was  $1.05 \pm 0.44$  ( $n=166$ ) at the MCD pole and  $5.57 \pm 2.67$  ( $n=166$ ) at the MCP (Fig. 3A and B). This latest value  
201 is similar to that measured for  $\Delta cotE$  sporangia with a refringent forespore (Fig. 3A). We concluded that MTG  
202 appears associated to a similar structure on the surface of  $\Delta cotE$  forespores and in the front region of partly  
203 engulfed forespore of WT10876 sporangia.

204 In parallel, we imaged by TEM sporulating engulfment-defective cells collected at hour 48, at the time  
205 we detected MTG bright/TMR-star signals (Fig. 4B). According to our SIM observations, we clearly observed  
206 cells with an incomplete engulfment and coat material present towards the leading edge of the mother cell  
207 engulfing membrane (Fig. 4B, yellow arrow, see also inset in the right panel), together with a smaller amount  
208 of coat material inside the mother cell cytoplasm (Fig. 4B, red arrows). In addition, we clearly observed  
209 abundant exosporium-like material closely associated with the coat material (Fig. 4B, pink arrows). MTG  
210 signals corresponding to exosporium were not observed by SIM in bearding sporangia (Fig. 4A, panels *d* and  
211 *e*), likely hidden by the bright MTG signal bound to the coat material very close to the exosporium. Detection  
212 of abundant exosporium material in the cytoplasm of the mother cell indicates that extension of the  
213 exosporium from the cap, usually observed concomitantly with coat deposition<sup>18,23,24</sup>, also occurs in  
214 engulfment-defective *B. cereus* cells. In agreement with this, we observed partial encasement of the forespore  
215 bulge by CotE-SNAP and formation of a continuous CotE-SNAP signal in apparent engulfment-defective cells  
216 with MTG bright signals (Supplementary Fig. S2, see also Materials and methods). Altogether, these results  
217 confirm our ability to assess faithfully by SIM the state of coat development in live sporangia.

218

219 **The TMR-star signal on the coat is  $\sigma^K$ -dependent.** A previous study reported the absence of coat in  $\Delta sigK$   
220 sporangia of a *B. cereus sensu lato* group strain (*B. thuringiensis* 407, WT407)<sup>55</sup>. Thus, if our TMR-star labelling  
221 faithfully reports the electron-dense coat material localization described by TEM, no TMR-star labelling  
222 should be observed in  $\Delta sigK$  sporangia. We imaged WT407 and  $\Delta sigK$  sporangia after dual labeling with TMR-  
223 star and MTG, using conventional epifluorescence and phase contrast microscopy (Fig. 5A-D, upper panels).  
224 Here we focused our analysis on TMR-star signals since MTG poorly distinguished coat once completely  
225 assembled in a WT condition (Fig. 3A, blue boxplots, compare also panels *d* and *g* in MTG channel of Fig. 2A).  
226 The characteristic ovoid TMR-star signal was observed covering the surface of most of WT407 refringent  
227 forespores at hour 24 (Fig. 5A, "No fusion", cyan arrows, see also the linescan profile in Fig. 5B), while it was  
228 undetected in  $\Delta sigK$  sporangia (Fig. 5C, see also the linescan profile in Fig. 5D). This result shows that  
229 detection of TMR-star signal on the forespore surface is  $\sigma^K$ -dependent.

230

231 **A SNAP fusion allows visualization of BxpB, a late exosporium protein.** In *B. cereus*, SNAP-fusions were  
232 particularly efficient to localize early assembling exosporium proteins such as CotE<sup>15</sup>, while a GFP fusion was  
233 not<sup>13</sup>. In addition, an attempt to localize a fusion of GFP to BxpB, a  $\sigma^K$ -dependent late assembling exosporium  
234 protein<sup>56</sup>, failed in *B. cereus*, while equivalent fusions were successfully visualized in *B. anthracis* and *B.*  
235 *megaterium*<sup>22,57</sup>. To check whether i) BxpB can be localized using a SNAP-fusion, ii) BxpB-SNAP-TMR-star  
236 signal can be distinguished from binding of TMR-star on coat fragments and iii)  $\sigma^K$  is active in engulfment-  
237 defective cells, we monitored by conventional fluorescence microscopy the detection of BxpB-SNAP in WT407

238 (Fig. 5A and B, middle panels), in a congenic  $\Delta sigK$  mutant (Fig. 5C and D, middle panels), in WT10876 (Fig.  
239 5E-G, middle panels) and in a congenic  $\Delta exsY$  (Fig. 5E-G, lower panels) during sporulation at 20°C. In the  
240 absence of ExsY, exosporium extension does not occur and only the exosporium MCP cap with sometimes a  
241 thinner MCD cap, both formed by CotY, are assembled<sup>15,20,25</sup>. Importantly, in  $\Delta exsY$  strains of *B. cereus* and *B.*  
242 *anthracis*, the exosporium MCP cap is less stably attached to the spore surface<sup>15,19,20,25</sup>. Hence, in engulfment-  
243 defective cells of a  $\Delta exsY$  strain, we expected to reduce the spatial proximity between exosporium and coat  
244 material to maximize our chance to distinguish eventual BxpB-SNAP-TMR-star signals from TMR-star-coat  
245 signals.

246 In *B. anthracis*, BxpB-mCherry and -GFP fusions are firstly detected at low level in the mother cell  
247 cytoplasm and ultimately localize as a ring around the forespore<sup>16,22</sup>. Accordingly, in addition to a  
248 characteristic ovoid TMR-star signal on the surface of refringent forespores and likely reflecting TMR-star  
249 binding to the coat (Fig. 5A and B, E and F, middle panels, cyan arrows), we observed a weak signal in the  
250 mother cell of WT407 and WT10876+BxpB-SNAP (Fig. 5A and B, E and F, middle panels, pink arrows and see  
251 red boxes in the linescan profiles). This signal was not observed in the absence of BxpB-SNAP (Fig. 5A and B,  
252 E and F, upper panels, "No fusion"). Later at hour 42, BxpB-SNAP displayed an exosporium localization  
253 (Supplementary Fig. S3) while no TMR-star signal was detected in  $\Delta sigK$ +BxpB-SNAP sporangia (Fig. 5C and  
254 D, middle panels, see also Supplementary Fig. S3). In contrast, the cap localization specific of the early  
255 assembling CotY-SNAP was observed in WT407 and  $\Delta sigK$  cells (Fig. 5A-D, lower panels, pink arrows and the  
256 linescans). Hence, together those results show that, despite the binding of TMR-star to the coat observed  
257 upon  $\sigma^k$  activation, a SNAP fusion allows the successful detection of a late assembling exosporium protein.

258 A weak TMR-star signal was observed in engulfment-defective WT10876+BxpB-SNAP cells (Fig. 5E  
259 and G, middle panels, red asterisks), however this signal was not specific from BxpB-SNAP since it was similar  
260 to the one observed in absence of the SNAP fusion (Fig. 5E and G, upper panels, orange arrows). In  $\Delta exsY$   
261 sporangia with a refringent forespore, in addition to a TMR-star signal on forespore surface (Fig. 5E and F,  
262 lower panels, cyan arrows), we observed a clear TMR-star signal specific of BxpB-SNAP drawing a cap-like  
263 structure towards the mother cell cytoplasm (Fig. 5E and F, lower panels, pink arrows). Bearding phenotypes  
264 were observed in  $\Delta exsY$  sporangia but less frequently than in WT10876 sporangia (14±4% versus 24±9%, Fig.  
265 5H). Importantly, similar cap-like localizations were also observed in engulfment-defective  $\Delta exsY$  cells,  
266 suggesting binding of TMR-star to the BxpB-SNAP fusion (Fig. 5E and G, red asterisks in bottom panels, pink  
267 arrows and the linescan). However, apparent MTG bright signals indicating presence of coat material are  
268 often detected closely associated to the cap-like TMR-star signal in the mother cell cytoplasm. Thus, based  
269 on these diffraction limited images, we cannot fully rule out the possibility that the coat material is more  
270 spread in the mother cell cytoplasm of  $\Delta exsY$  engulfment defective cells.

271



272 **BxpB-SNAP is specifically detected in engulfment-defective sporangia.** To determine whether a specific  
273 TMR-star signal of BxpB-SNAP can be distinguished from TMR-star binding to coat material in engulfment-  
274 defective  $\Delta exsY$  cells, we designed a quantitative co-localization analysis of TMR-star and MTG signals (Fig.  
275 6, see Materials and methods). We reasoned that signal originating from TMR-star bound on coat fragments  
276 should co-localize with MTG brighter signals, while a specific BxpB-SNAP-TMR-star signal should not. We  
277 performed this co-localization analysis on high-resolution lattice-SIM images of spores, of exosporium cap  
278 and of engulfment-defective  $\Delta exsY$  cells showing brighter MTG signals (“bearding”) (Fig. 6A and B). We used  
279  $\Delta exsY$  cells without SNAP-fusion (No fusion) to monitor the co-localization of TMR-star and MTG signals due  
280 to their binding on coat fragments and  $\Delta exsY$ +CotY-SNAP cells, as a positive control of a specific exosporium  
281 TMR-star binding.

282 In  $exsY$  spores without SNAP fusion, TMR-star and MTG signals largely co-localized in the central  
283 region of the spore (grey in panel a, Fig. 6A), with a Pearson’s correlation coefficient “ $r$ ” of  $0.74 \pm 0.07$  ( $n=63$ )  
284 (Fig. 6B). In contrast, the TMR-star signal did not co-localize with the MTG signal around the forespore in  
285  $\Delta exsY$ +CotY-SNAP spores (Fig. 6A panel *d*,  $r=0.02 \pm 0.10$ ,  $n=92$ ) and appeared instead preferentially  
286 associated with the cap(s) (Fig. 6A and 6B). Accordingly, when looking exclusively at the exosporium cap, the  
287 TMR-star signal co-localized with the MTG for  $\Delta exsY$ +CotY-SNAP (panel *e*,  $r=0.67 \pm 0.19$ ,  $n=100$ ), while a  
288 random distribution of the correlation coefficient ( $r=0.31 \pm 0.25$ ,  $n=110$ ) is observed in  $\Delta exsY$  spores without  
289 fusion (panel *b*). Importantly, the TMR-star signal did not co-localize with the MTG in  $\Delta exsY$ +CotY-SNAP  
290 bearding sporangia (panel *f*,  $r=-0.16 \pm 0.14$ ,  $n=16$ ), in contrast to  $\Delta exsY$  sporangia without fusion (panel *c*,  
291  $r=0.83 \pm 0.21$ ,  $n=42$ ). Hence, the CotY-SNAP-TMR-star signal can be specifically distinguished from the TMR-  
292 star binding to the coat material in  $\Delta exsY$  engulfment-defective sporangia.

293 The analysis of  $\Delta exsY$ +BxpB-SNAP cells shows that the TMR-star signal co-localized with MTG signal  
294 in spores ( $r=0.69 \pm 0.16$ ,  $n=113$ , panel *g* in Fig. 6A, and 6B) but not in the exosporium cap of spores (panel *h*,  
295  $r=0.07 \pm 0.26$ ,  $n=63$ ). Interestingly, in this latest condition, the TMR-star appears often associated with the  
296 margin of the exosporium cap, a particular pattern of localization which was recently reported by an  
297 immunofluorescence analysis of BxpB in *B. anthracis*  $\Delta exsY$  mutant spores<sup>19</sup>. In sporangia showing the  
298 “bearding” phenotype, we observed a strong TMR-star signal which did not co-localize with MTG (panel *i*,  
299  $r=-0.01 \pm 0.19$ ,  $n=35$ ). We concluded that the TMR-star signal observed in  $\Delta exsY$ +BxpB-SNAP engulfment-  
300 defective sporangia that does not colocalize with MTG, reveals the specific binding of TMR-star on BxpB-  
301 SNAP.

302 We also acquired Z-stack images of the coat fragments released by the lysis of bearding cells using  
303 lattice-SIM (Fig. 6C). On maximum projections of Z-stack images, we clearly recognized specific TMR-star  
304 signal of CotY- and BxpB-SNAP fusions (in magenta) in the 3D space drawn by coat fragments (in green)  
305 labeled by the MTG (Fig. 6C). In contrast, in  $\Delta exsY$  without fusion, the TMR-star signal is only viewed

306 superimposed on MTG signals. This analysis also showed a specific TMR-star signal due to BxpB-SNAP,  
307 associated to the fragments released after the lysis of bearding WT10876 sporangia (Fig. 6C). In this latest  
308 condition, the BxpB-SNAP-TMR-star signal appears closely associated to the curved coat fragments. Taken  
309 together, both the nanoscale co-localization analysis and super-resolved Z-maximum projection images  
310 demonstrate the presence of a TMR-star signal specific of BxpB-SNAP in engulfment-defective *B. cereus* cells,  
311 suggesting that  $\sigma^K$  is active in these cells.

312

## 313 Discussion

314 Determination of the state of coat and exosporium development in sporangia or in spores is an  
315 unavoidable step in developmental studies of *B. cereus*. To date, this was largely performed by TEM. We  
316 recently showed that MTG labeling allows to directly observe the basal layer of the exosporium cap after  
317 engulfment completion and the following steps of exosporium formation using SIM<sup>15</sup>. Here, we demonstrated  
318 that both TMR-star and MTG specifically stain the coat of *B. cereus*, and that SIM reconstructed signals can  
319 be used to assess the precise stages of coat development. Thus, it is now possible using these fluorescence  
320 markers to determine the precise stage of both exosporium and coat assembly in living cells using  
321 fluorescence microscopy, without the need for genetic manipulations. Since DNA recombination is poorly  
322 effective and the genetic toolbox is limited for *B. cereus* species compared to other *Bacilli*<sup>11,12</sup>, we believe that  
323 our non-genetic fluorescence live imaging approach could be particularly efficient to characterize  
324 mechanisms of proteinaceous spore surface layers assembly in new *B. cereus* isolates or to assess the effect  
325 of destruction treatments at the cell level. Notably, we showed that binding of TMR-star to the coat gives a  
326 characteristic ovoid signal around the forespore in WT14579, WT10876 and WT407 strains. Two of those  
327 strains are *B. cereus sensu stricto* species while WT407 is a *B. thuringiensis* strain. Hence, we assume that our  
328 results are valid for other species of the *B. cereus sensu lato* group and notably for *B. anthracis* strains.

329 Although TMR-star and MTG both bind to the coat, the detected signals differ due to the ability of  
330 MTG to bind also to the cell's membranes and exosporium, while TMR-star only binds to the coat.  
331 Interestingly, the signal originating from TMR-star binding the coat could still be detected in some strains  
332 expressing SNAP-fusions. Notably, in cells expressing BxpB-SNAP, binding of TMR-star to the coat firstly  
333 represents most of the TMR-star signal observed (Fig. 5A and B, middle panels). In a WT strain expressing  
334 CotE-, CotY- or ExsY-SNAP fusions, such TMR-star association with the forespore surface was not  
335 distinguishable at any stage of the sporulation<sup>15</sup>. Encasement by those morphogenetic proteins is completed  
336 soon after engulfment completion and before the forespore becomes refringent, and the strong signal of  
337 these fusions in vicinity of the forespore surface likely masks the weak TMR-star signal coming from binding  
338 to the coat. In agreement with this statement, the TMR-star association with the forespore surface can be  
339 observed when localization of CotY-SNAP is impaired, as observed in  $\Delta cotE$ ,  $\Delta exsY$ <sup>15</sup> and in WT407 strains

340 (Fig. 5A-B, lower panels). Hence, our studies indicate that TMR-star cannot be used as a coat marker in strains  
341 expressing abundant early assembling SNAP-tag exosporium proteins. In such strains, bright MTG signals  
342 reconstructed by SIM and observed at intermediate stages of coat deposition or in cells showing coat  
343 assembly defects can be used as spatial and temporal markers of coat development.

344 In this study, we also find that the coat appears less permeable to MTG when completely covering  
345 the forespore surface, as judged by a complete ovoid TMR-star signal observed in such cells and in free  
346 spores. We also noticed that the coat material accessibility to MTG is higher in  $\Delta cotE$  sporangia, including  
347 those with a forespore fully covered by a TMR-star signal, suggesting that coat permeability is affected among  
348 the whole population of  $\Delta cotE$  sporangia. Hence, the high sensitivity to lysozyme reported for  $\Delta cotE$  spores  
349 formed at 20°C<sup>47</sup> may not only be due to the partly decoated spores, as observed by TEM. A recent report  
350 indicates that CotG, a CotE-controlled protein of *B. subtilis* (ExsB is a homologue in *B. cereus*<sup>58,59</sup>), and a  
351 central determinant of outer coat patterning<sup>60-63</sup>, mediates spore permeability<sup>64</sup>. Thus, it is tempting to  
352 suggest that a defect in ExsB assembly may explain the apparent increase accessibility of the coat in *B. cereus*  
353  $\Delta cotE$  cells formed at suboptimal temperature. Our observations show that the quantification of the MTG  
354 signals is a promising tool to evaluate the structuration state and likely the permeability of the coat directly  
355 at the single cell level.

356 We applied our super-resolved SIM-based fluorescent analysis to characterize the proteinaceous  
357 spore surface layers development in a heterogeneous population, observed when sporulation *B. cereus* ATCC  
358 10876 cells occurs at 20°C. We confirmed a complete arrest of the engulfment process in a variable part of  
359 the cells, with: i) a dual labeling of cell's membrane with MTG and FM4-64, ii) a TEM analysis and iii) a  
360 quantification of MTG fluorescence signals. Engulfment defects observed were characterized by a bulging of  
361 the forespore towards the mother cell cytoplasm. These bulging cells never became refringent and ultimately  
362 lysed, indicating a failure in the forespore development. Importantly, despite an incomplete engulfment, we  
363 characterized multiple features normally observed only in engulfed cells; i) synthesis and accumulation of  
364 coat material close to the forespore bulge, creating a coat bearding phenotype, ii) partial encasement by  
365 CotE-SNAP, iii) exosporium extension and iv) synthesis of BxpB-SNAP fusion. Except the encasement by CotE-  
366 SNAP, the other features are governed by the late mother-cell specific  $\sigma^K$  factor. Altogether, our results  
367 suggest that  $\sigma^K$  is active in engulfment-defective WT10876 cells.

368 Strikingly, the coat bearding phenotype reported here in engulfment-defective *B. cereus* cells, is  
369 reminiscent of the one described in engulfment-defective *C. difficile* sporangia<sup>35</sup>. Bearding phenotype in *C.*  
370 *difficile* likely originates from the absence of an inhibitory  $\sigma^K$  pro-sequence<sup>29</sup>. In *B. cereus* genomes, a  $\sigma^K$  pro-  
371 sequence and associated protease are present<sup>65</sup>. However, in most of the *B. cereus* species, an interrupting  
372 *skin* element and the associated SpoIVCA recombinase are absent<sup>66,67</sup>. Thus, *B. cereus* and *C. difficile* had  
373 evolved different strategies leading to a less tight regulation of  $\sigma^K$  activation. Importantly, since modulation

374 in  $\sigma^K$  activation control has been only demonstrated in pathogenic species, one can suggest that  $\sigma^K$  activity  
375 in engulfment-defective cells may confer an advantage in the context of an infection. An appealing possibility  
376 is that the formation and release of partially structured materials of the proteinaceous spore surface may be  
377 the way to expose to the media/the host, internal components otherwise never exposed. Such exposition  
378 may create new interactions with the immune system, to dupe it and/or to generate a particular matrix for  
379 the normally assembled spores.

380

## 381 **Materials and methods**

382 **Bacterial strains, plasmids and general methods.** Strains and plasmids used in this study are listed in Table  
383 1. The various fluorescent fusions are carried by the low copy pHT304-18 plasmid and described in Table 1.  
384 The *bxpB-SNAP* gene fusion was synthesized by ATUM ([www.atum.bio](http://www.atum.bio), Newark, CA). Briefly, synthetic inserts  
385 corresponding to the *bxpB* gene (bc\_1221) and the 169 bp sequence upstream of the *bxpB* start codon of *B.*  
386 *cereus* ATCC 14579, followed by a GCAGCTGCT linker and the SNAP sequence were inserted into the pHT304-  
387 18 plasmid, using *Sa*I and *Eco*RI restriction sites, giving rise to the pHT304-BxpB-SNAP (Table 1). All plasmids  
388 were first introduced into *E. coli* DH5 $\alpha$  and clones were confirmed by PCR and/or DNA sequencing. Plasmids  
389 were then transferred to *E. coli* SCS110; the resulting unmethylated plasmids were then transferred to the *B.*  
390 *cereus*/*B. thuringiensis* strains by electroporation. LB agar plates or LB broth with orbital shaking (200 rpm)  
391 were used for routine growth at 37°C. When needed, liquid cultures or plates were supplemented with the  
392 following antibiotics at the indicated concentrations: ampicillin (Amp) at 100mg·ml<sup>-1</sup> for *E. coli* cultures,  
393 spectinomycin (Spc) at 275mg·ml<sup>-1</sup>, kanamycin (Kan) at 200mg·ml<sup>-1</sup> and erythromycin (Erm) at 5mg·ml<sup>-1</sup> for  
394 *B. cereus* and *B. thuringiensis* cultures. Sporulation was induced by resuspension in liquid SMB medium at  
395 20°C with orbital shaking at 180 rpm, as previously described<sup>15</sup>.

396

397 **SNAP labeling and fluorescence microscopy.** Samples (1mL) were withdrawn from cultures in SMB at  
398 selected times during sporulation. Cells were collected by centrifugation (10,000 x g for 3 min), resuspended  
399 in 200  $\mu$ L of phosphate saline buffer (PBS) and labeled by incubation with SNAP-cell TMR-Star (New England  
400 Biolabs) for 30 min at 37°C in the dark at a final concentration of 250 nM. This TMR-star-probed suspension  
401 was centrifuged (12,000 x g, 1 min), washed with 1 mL of PBS, suspended again in 1mL of PBS and labeled  
402 with Mitotracker Green (MTG, Thermofischer) and/or FM4-64 Fx at a final concentration of 1  $\mu$ g/mL or in 100  
403 nM MV405 for simultaneous visualization of YFP protein (Supplementary Fig. S3) for 1 min at room  
404 temperature. Cells were then washed three times in PBS and suspended in 50 $\mu$ L to 200  $\mu$ L PBS, depending  
405 on the concentration of sporulating cells/spores. For diffraction-limited as well as super-resolved microscopy,  
406 3  $\mu$ L of the labeled cells suspension were applied onto 1.7% agarose in PBS-coated glass slides. All

407 experiments were done at RT. Samples were imaged with a BX-61 (Olympus), Elyra PS.1 or Elyra 7  
408 AxioObserver (Zeiss) microscope.

409

410 **Microscopy acquisition settings.** Samples were observed with an epifluorescence microscope (BX-61;  
411 Olympus) equipped with an Olympus UPlanFL N 100x/1.30 Oil Microscope Objective, an Orca Flash 4.0 LT  
412 camera (Hamamatsu) and illuminated by a fluorescence LED lamp (PE300 WHT-365). Images were acquired  
413 using the CellSens Olympus software, for TMR-star acquisitions exposure time was 500ms for all images and  
414 31ms for MTG acquisitions. Final pixel size was 65 nm for raw image. Super Resolution Structured Illumination  
415 Microscopy (SIM)<sup>68</sup> images were acquired using an Elyra PS.1 Microscope (Zeiss) equipped with a Plan-  
416 Apochromat 63x/1.4 oil DIC M27 objective and a Pco. edge 5.5 camera, using 488 nm (100mW) or 561 nm  
417 (100 mW) laser lines, at 15% and 10% of total potency for 488 and 561 nm lasers respectively. Final pixel size  
418 was 64.5 nm for raw image. The grid periods used were 28 nm or 34 nm for acquisitions with the 488 nm or  
419 561 nm lasers respectively. For each SIM acquisition, the corresponding grating was shifted and rotated five  
420 times, giving 25 acquired frames. Final SIM images were reconstructed using the ZEN software (black edition,  
421 2012, version8, 1, 0, 484; Zeiss), using synthetic, channel-specific Optical Transfer Functions (OTFs), baseline  
422 cut and noise filter settings ranging from -7 to -8. Lattice SIM imaging was performed on a Zeiss Elyra 7  
423 AxioObserver inverted microscope equipped with 488 nm (100 mW), 561 nm (100 mW), and 642 nm  
424 (150 mW) laser lines, at 20% of maximal output power, a sCMOS camera (PCO Edge edge 4.2), a 63x/NA 1.4  
425 objective (Zeiss, Plan-Apochromat 63x/1.4 Oil DIC M27) and an additional lens (1.6x) in the detection pathway.  
426 Final pixel size was 64.5 nm for raw image. The fluorescence emission was separated from the laser excitation  
427 by a dichroic beamsplitter (405/488/561/641) and filtered (dual band with two bandpass 495-550 and 570-  
428 620) before detection. Image acquisition was controlled by the Zen Software (Zeiss, black edition). The Lattice  
429 SIM approach is based on stands on an illumination of point pattern<sup>69,70</sup> and laterally shifted patterns on the  
430 sample (called phase images). The raw images were composed of 15 phase images per plane per channel,  
431 and acquired with a Z-distance of 0.100  $\mu\text{m}$ . The grids were chosen to be optimal for both laser lines and  
432 modulation contrast (27.5 and 32  $\mu\text{m}$  grids for the 488 and 561 laser lines respectively). The lattice SIM  
433 reconstruction was performed with Zen software with automatic settings, baseline cut and sharpness settings  
434 ranging from 7 to 9. Negative values resulting from SIM processing (due to the sharpness filter) were clipped  
435 by setting them to zero. The intensities of final reconstructed SIM images were normalized to the maximum  
436 dynamic range to be displayed with optimal brightness and contrast. For all exposure time was 20 ms.

437

438 **Image analysis.** All image analysis were performed and micrographs processed using Fiji software  
439 (ImageJ, NIH). Brightness and contrast of representative cell images were adapted in Fiji and figures were  
440 compiled using Inkscape 0.92.5. (<https://inkscape.org>). At least three different microscopic fields were  
441 analyzed for every condition.

442 **(i) Quantification of MTG signal ratio intensity between the forespore and the mother cell.** The  
443 sporulation stages were determined with brightfield (BF) and MTG channels. First, on SIM reconstructed  
444 images, one polygonal region of interest (ROI) was adjusted using the Fiji polygon tool on the forespore (FS)  
445 membrane and a second ROI was positioned on the mother cell (MC) membrane of the same sporangia. The  
446 polygonal ROI were transferred on pseudo-widefield images and the mean intensity in the two ROI were  
447 recorded and an individual FS/MC was computed for every sporangium. This method was repeated for the  
448 indicated numbers of sporangia. At least two biological replicates were used per condition. We used  
449  $\Delta cotE$ +CotY-SNAP SIM images previously acquired in the same condition<sup>15</sup> as a second replicate for  
450 quantification of FS/MC MTG ratio in  $\Delta cotE$  cells. Since assembly of CotY-SNAP is blocked in  $\Delta cotE$  cells, a  
451 minimal impact of CotY-SNAP synthesis on coat deposition is attempted. To increase the size of our statistical  
452 sampling of engulfment-defected cells, we used sporangia in different ATCC 10876 backgrounds, showing  
453 engulfment defects that we used in the course of the present study. Hence results presented in Fig. 3A  
454 included ratio computed for WT10876, WT10876+CotE-SNAP,  $\Delta exsY$ ,  $\Delta exsY$ +CotE-SNAP strains.

455 **(ii) Quantification of interspace size on SIM images.** The distance separating the basal layer of the  
456 exosporium cap from the underlying outer forespore membrane (OFM) was calculated in MTG channel of  
457 SIM images using the Fiji function 'points to distance'. Only sporangia with an apparent exosporium cap in  
458 the focal plan were used. The distance was calculated between the exosporium cap point at the maximum  
459 distance from the surface of the forespore and the center of the MCP pole of the forespore.

460 **(iii) Counting of sporangia and spores with defects of coat assembly.** SIM images of sporangia  
461 of refringent spores (black in BF images) from two biological replicates of WT cells collected at hour 24 or  
462  $\Delta cotE$  and  $\Delta cotE$  expressing CotY-SNAP cells, collected at hour 48 or spores collected at hour 72 were used  
463 for analysis. The  $\Delta cotE$  cells presented a delay of sporulation and none of the engulfed sporangia observed  
464 at hour 24 was refringent or showed TMR-star/MTG brighter signals. Normal patterns of MTG brighter signals  
465 localization were defined according to previous TEM study<sup>15,18,23</sup> and as presented in Fig. 1.

466 **(iv) Quantification of TMR-star signal in the forespore.** Quantification was adapted from Delerue  
467 et al<sup>71</sup>. To determine the proportion of TMR-star signal associated with the forespore among the sporangia,  
468 a polygonal ROI was first fitted on the forespore region and a second ROI was positioned on the sporangia  
469 outline in the TMR-star channel of diffraction-limited images. For  $\Delta sigK$  sporangia, since forespore did not  
470 become refringent, we adjusted ROI on engulfed cells with phase black/phase grey forespore. The total  
471 fluorescence was recorded in the forespore ( $F_{FS}$ ) and in the sporangium ( $F_{sporangium}$ ). The forespore signal was  
472 computed for individual sporangia as follow:  $(F_{FS}-F_{background}) \times 100 / (F_{sporangium}-F_{background})$ . The mean  
473 fluorescence of the image signal background ( $F_{background}$ ) was adjusted for every microscopy field.

474 **(v) Quantification of sporangia showing a coat bearding phenotype among the sporulating**  
475 **population on diffraction-limited images.** The proportion of sporangia showing a bearding phenotype at

476 hour 48 among the global sporulating population was determined by identifying cells with a red TMR-star  
477 signal, an apparent forespore bulging as judged by MTG labelling and not appearing bright or grey in phase  
478 contrast microscopy. Biological triplicates were used for W10876+BxpB-SNAP and  $\Delta exsY$ +BxpB-SNAP cells.

479 **(vi) Quantification of Pearson correlation coefficient on Lattice-SIM images.** Co-localization of  
480 MTG with TMR-star signals on lattice-SIM reconstructed images (see "Microscopy acquisition settings  
481 section") was assessed by the Colocalization Threshold plugin<sup>72</sup> available on Fiji. The co-localization  
482 coefficient was recorded in different regions defined using the polygon tool of Fiji in MTG channel and  
483 encompassing, (i) the entire spores including the associated cap(s), (ii) only the biggest cap or (iii) the contour  
484 of the sporangia showing a bearding phenotype. Pearson's correlation coefficient was calculated for  
485 individual regions, with a coefficient value of 1 representing a perfect positive linear correlation and a value  
486 of 0 indicating an absence of correlation. When no correlation was found by the function, a score of -0.2 was  
487 assigned.

488 **(vii) Quantification of TMR-star signal length.** Quantification was performed on SIM reconstructed  
489 images (Supplementary Fig. S2C and D). Using Fiji program, a segmented line was fitted from one end to the  
490 other of the layer drawn by the TMR-star signal. For CotE-SNAP, additional, weakest layers were often  
491 observed. Quantification was only performed on the layer closest from the forespore bulge. The length of the  
492 line, used as a proxy of encasement by CotE-SNAP and CotY-SNAP was determined in the different sporangia  
493 classified using bright field and MTG fields. Sporangia showing an apparent forespore bulging, a FS/MC MTG  
494 signal ratio towards the MCD pole  $<1.2$ , were defined as "bulging" cells and those showing, in addition, MTG  
495 bright signals towards the bulge, *i.e.* a FS/MC MTG ratio  $>3$ , were defined as "bearding" cells.

496

497 **Transmission electron microscopy.** Samples from SMB cultures were collected by centrifugation 48 h after  
498 the onset of sporulation, and the cells fixed and processed for thin sectioning TEM as described before<sup>15</sup>.

499

500 **Statistics.** Statistical analyses were performed using Rstudio version 4.1.1 for PC. Data are represented with  
501 boxplots showing the interquartile range (25<sup>th</sup> and 75<sup>th</sup> percentile). The upper whisker extends from the hinge  
502 to the largest value no further than 1.5 x IQR from the hinge and the lower whisker extends from the hinge  
503 to the smallest value at most 1.5 x IQR of the hinge. All sporulation kinetics were replicated at least twice  
504 using conventional fluorescence microscopy before being imaged by SIM or lattice SIM. The number of cells  
505 analyzed is indicated in each figure.

506

#### 507 **Data availability**

508 The datasets used and/or analyzed during the current study are available from the corresponding author on  
509 reasonable request.

## 510 **References**

- 511 1. Henriques, A. O. & Moran, C. P., Jr. Structure, Assembly, and Function of the Spore Surface Layers.  
512 *Annual Review of Microbiology* **61**, 555–588 (2007).
- 513 2. Stewart, G. C. The Exosporium Layer of Bacterial Spores: a Connection to the Environment and the  
514 Infected Host. *Microbiol. Mol. Biol. Rev.* **79**, 437–457 (2015).
- 515 3. Khanna, K., Lopez-Garrido, J. & Pogliano, K. Shaping an Endospore: Architectural Transformations  
516 During *Bacillus subtilis* Sporulation. *Annu Rev Microbiol* **74**, 361–386 (2020).
- 517 4. Walker, P. D. (Symposium on Bacterial Spores: Paper I). Cytology of Spore Formation and  
518 Germination. *Journal of Applied Bacteriology* **33**, 1–12 (1970).
- 519 5. Cavalcante, D. de A. *et al.* Ultrastructural analysis of spores from diverse Bacillales species isolated  
520 from Brazilian soil. *Environmental Microbiology Reports* **11**, 155–164 (2019).
- 521 6. Driks, A. & Eichenberger, P. The Spore Coat. in *The Bacterial Spore* 179–200 (John Wiley & Sons, Ltd,  
522 2016). doi:10.1128/9781555819323.ch9.
- 523 7. Browne, H. P. *et al.* Culturing of ‘unculturable’ human microbiota reveals novel taxa and extensive  
524 sporulation. *Nature* **533**, 543–546 (2016).
- 525 8. Lehmann, D. *et al.* Role of novel polysaccharide layers in assembly of the exosporium, the outermost  
526 protein layer of the *Bacillus anthracis* spore. *Molecular Microbiology* **118**, 258–277 (2022).
- 527 9. McKenney, P. T., Driks, A. & Eichenberger, P. *The Bacillus subtilis* endospore: assembly and functions  
528 of the multilayered coat. *Nature Reviews Microbiology* **11**, 33–44 (2013).
- 529 10. Riley, E. P., Schwarz, C., Derman, A. I. & Lopez-Garrido, J. Milestones in *Bacillus subtilis* sporulation  
530 research. *Microb Cell* **8**, 1–16.
- 531 11. Eijlander, R. T. & Kuipers, O. P. Live-Cell Imaging Tool Optimization To Study Gene Expression Levels  
532 and Dynamics in Single Cells of *Bacillus cereus*. *Applied and Environmental Microbiology* **79**, 5643–5651  
533 (2013).
- 534 12. Arnaud, M., Chastanet, A. & Débarbouillé, M. New Vector for Efficient Allelic Replacement in  
535 Naturally Nontransformable, Low-GC-Content, Gram-Positive Bacteria. *Applied and Environmental*  
536 *Microbiology* **70**, 6887–6891 (2004).
- 537 13. Ghosh, A. *et al.* Proteins Encoded by the gerP Operon Are Localized to the Inner Coat in *Bacillus*  
538 *cereus* Spores and Are Dependent on GerPA and SafA for Assembly. *Appl. Environ. Microbiol.* **84**, (2018).
- 539 14. Motomura, K. *et al.* The C-Terminal Zwitterionic Sequence of CotB1 Is Essential for Biosilicification of  
540 the *Bacillus cereus* Spore Coat. *Journal of Bacteriology* **198**, 276–282 (2016).
- 541 15. Lablaine, A. *et al.* The Morphogenetic Protein CotE Positions Exosporium Proteins CotY and ExsY  
542 during Sporulation of *Bacillus cereus*. *mSphere* **6**, (2021).



- 543 16. Thompson, B. M., Hsieh, H.-Y., Spreng, K. A. & Stewart, G. C. The co-dependence of BxpB/ExsFA and  
544 BclA for proper incorporation into the exosporium of *Bacillus anthracis*. *Molecular Microbiology* **79**, 799–  
545 813 (2011).
- 546 17. Thompson, B. M., Hoelscher, B. C., Driks, A. & Stewart, G. C. Assembly of the BclB glycoprotein into  
547 the exosporium and evidence for its role in the formation of the exosporium 'cap' structure in *Bacillus*  
548 *anthracis*. *Molecular Microbiology* **86**, 1073–1084 (2012).
- 549 18. Boone, T. J. *et al.* Coordinated Assembly of the *Bacillus anthracis* Coat and Exosporium during  
550 Bacterial Spore Outer Layer Formation. *mBio* **9**, (2018).
- 551 19. Durand-Heredia, J., Hsieh, H.-Y., Spreng, K. A. & Stewart, G. C. Roles and Organization of BxpB  
552 (ExsFA) and ExsFB in the Exosporium Outer Basal Layer of *Bacillus anthracis*. *Journal of Bacteriology* **0**,  
553 e00290-22 (2022).
- 554 20. Durand-Heredia, J., Hsieh, H.-Y., Thompson, B. M. & Stewart, G. C. ExsY, CotY, and CotE Effects on  
555 *Bacillus anthracis* Outer Spore Layer Architecture. *Journal of Bacteriology* **204**, e00291-22 (2022).
- 556 21. Durand-Heredia, J. & Stewart, G. C. Localization of the CotY and ExsY proteins to the exosporium  
557 basal layer of *Bacillus anthracis*. *MicrobiologyOpen* **11**, e1327 (2022).
- 558 22. Giorno, R. *et al.* Localization and assembly of proteins comprising the outer structures of the *Bacillus*  
559 *anthracis* spore. *Microbiology (Reading)* **155**, 1133–1145 (2009).
- 560 23. Ohye, D. F. & Murrell, W. G. Exosporium and Spore Coat Formation in *Bacillus cereus* T. *Journal of*  
561 *Bacteriology* **115**, 1179–1190 (1973).
- 562 24. Giorno, R. *et al.* Morphogenesis of the *Bacillus anthracis* Spore. *Journal of Bacteriology* **189**, 691–  
563 705 (2007).
- 564 25. Boydston, J. A., Yue, L., Kearney, J. F. & Turnbough, C. L. The ExsY Protein Is Required for Complete  
565 Formation of the Exosporium of *Bacillus anthracis*. *Journal of Bacteriology* **188**, 7440–7448 (2006).
- 566 26. Johnson, M. J. *et al.* ExsY and CotY Are Required for the Correct Assembly of the Exosporium and  
567 Spore Coat of *Bacillus cereus*. *Journal of Bacteriology* **188**, 7905–7913 (2006).
- 568 27. Ryter, A. [Morphologic Study Of The Sporulation Of *Bacillus Subtilis*]. *Ann Inst Pasteur (Paris)* **108**,  
569 40–60 (1965).
- 570 28. Al-Hinai, M. A., Jones, S. W. & Papoutsakis, E. T. The Clostridium Sporulation Programs: Diversity and  
571 Preservation of Endospore Differentiation. *Microbiology and Molecular Biology Reviews* **79**, 19–37 (2015).
- 572 29. Fimlaid, K. A. & Shen, A. Diverse mechanisms regulate sporulation sigma factor activity in the  
573 Firmicutes. *Current Opinion in Microbiology* **24**, 88–95 (2015).
- 574 30. Kroos, L., Zhang, B., Ichikawa, H. & Yu, Y.-T. N. Control of  $\sigma$  factor activity during *Bacillus subtilis*  
575 sporulation. *Molecular Microbiology* **31**, 1285–1294 (1999).

- 576 31. Piggot, P. J. & Hilbert, D. W. Sporulation of *Bacillus subtilis*. *Current Opinion in Microbiology* **7**, 579–  
577 586 (2004).
- 578 32. Serrano, M. *et al.* Dual-Specificity Anti-sigma Factor Reinforces Control of Cell-Type Specific Gene  
579 Expression in *Bacillus subtilis*. *PLOS Genetics* **11**, e1005104 (2015).
- 580 33. Campo, N. & Rudner, D. Z. SpoIVB and CtpB Are Both Forespore Signals in the Activation of the  
581 Sporulation Transcription Factor  $\sigma^K$  in *Bacillus subtilis*. *Journal of Bacteriology* **189**, 6021–6027 (2007).
- 582 34. Serrano, M. *et al.* The SpoIIQ-SpoIIIAH complex of *Clostridium difficile* controls forespore  
583 engulfment and late stages of gene expression and spore morphogenesis. *Molecular Microbiology* **100**,  
584 204–228 (2016).
- 585 35. Fimlaid, K. A., Jensen, O., Donnelly, M. L., Siegrist, M. S. & Shen, A. Regulation of *Clostridium difficile*  
586 Spore Formation by the SpoIIQ and SpoIIIA Proteins. *PLOS Genetics* **11**, e1005562 (2015).
- 587 36. Saujet, L. *et al.* Genome-Wide Analysis of Cell Type-Specific Gene Transcription during Spore  
588 Formation in *Clostridium difficile*. *PLOS Genetics* **9**, e1003756 (2013).
- 589 37. Pereira, F. C. *et al.* The Spore Differentiation Pathway in the Enteric Pathogen *Clostridium difficile*.  
590 *PLOS Genetics* **9**, e1003782 (2013).
- 591 38. Fimlaid, K. A. *et al.* Global Analysis of the Sporulation Pathway of *Clostridium difficile*. *PLOS Genetics*  
592 **9**, e1003660 (2013).
- 593 39. Terry, C. *et al.* Molecular tiling on the surface of a bacterial spore – the exosporium of the *Bacillus*  
594 *anthracis/cereus/thuringiensis* group. *Molecular Microbiology* **104**, 539–552 (2017).
- 595 40. Stewart, G. C. Assembly of the outermost spore layer: pieces of the puzzle are coming together.  
596 *Molecular Microbiology* **104**, 535–538 (2017).
- 597 41. Cassona, C. P., Pereira, F., Serrano, M. & Henriques, A. O. A Fluorescent Reporter for Single Cell  
598 Analysis of Gene Expression in *Clostridium difficile*. in *Clostridium difficile: Methods and Protocols* (eds.  
599 Roberts, A. P. & Mullany, P.) 69–90 (Springer, 2016). doi:10.1007/978-1-4939-6361-4\_6.
- 600 42. Lanzilli, M. *et al.* The Exosporium of *Bacillus megaterium* QM B1551 Is Permeable to the Red  
601 Fluorescence Protein of the Coral *Discosoma* sp. *Frontiers in Microbiology* **7**, (2016).
- 602 43. Donadio, G., Lanzilli, M., Sirec, T., Ricca, E. & Istatico, R. Localization of a red fluorescence protein  
603 adsorbed on wild type and mutant spores of *Bacillus subtilis*. *Microbial Cell Factories* **15**, 153 (2016).
- 604 44. Sirec, T., Benarroch, J. M., Buffard, P., Garcia-Ojalvo, J. & Asally, M. Electrical Polarization Enables  
605 Integrative Quality Control during Bacterial Differentiation into Spores. *iScience* **16**, 378–389 (2019).
- 606 45. Magge, A., Setlow, B., Cowan, A. E. & Setlow, P. Analysis of dye binding by and membrane potential  
607 in spores of *Bacillus* species. *Journal of Applied Microbiology* **106**, 814–824 (2009).

- 608 46. Kuwana, R., Yamazawa, R., Ito, K. & Takamatsu, H. Comparative analysis of thioflavin T and other  
609 fluorescent dyes for fluorescent staining of *Bacillus subtilis* vegetative cell, sporulating cell, and mature  
610 spore. *Bioscience, Biotechnology, and Biochemistry* **87**, 338–348 (2023).
- 611 47. Bressuire-Isoard, C., Bornard, I., Henriques, A. O., Carlin, F. & Broussolle, V. Sporulation Temperature  
612 Reveals a Requirement for CotE in the Assembly of both the Coat and Exosporium Layers of *Bacillus cereus*  
613 Spores. *Appl. Environ. Microbiol.* **82**, 232–243 (2016).
- 614 48. Sharp, M. D. & Pogliano, K. An in vivo membrane fusion assay implicates SpoIIIIE in the final stages  
615 of engulfment during *Bacillus subtilis* sporulation. *PNAS* **96**, 14553–14558 (1999).
- 616 49. Doan, T. *et al.* FisB mediates membrane fission during sporulation in *Bacillus subtilis*. *Genes Dev.* **27**,  
617 322–334 (2013).
- 618 50. Perez, A. R., Mello, A. A.-D. & Pogliano, K. SpoIIB Localizes to Active Sites of Septal Biogenesis and  
619 Spatially Regulates Septal Thinning during Engulfment in *Bacillus subtilis*. *Journal of Bacteriology* **182**,  
620 1096–1108 (2000).
- 621 51. Mello, A. A.-D., Sun, Y.-L., Aung, S. & Pogliano, K. A cytoskeleton-like role for the bacterial cell wall  
622 during engulfment of the *Bacillus subtilis* forespore. *Genes Dev.* **16**, 3253–3264 (2002).
- 623 52. Meyer, P., Gutierrez, J., Pogliano, K. & Dworkin, J. Cell wall synthesis is necessary for membrane  
624 dynamics during sporulation of *Bacillus subtilis*. *Molecular Microbiology* **76**, 956–970 (2010).
- 625 53. Ojkic, N., López-Garrido, J., Pogliano, K. & Endres, R. G. Cell-wall remodeling drives engulfment  
626 during *Bacillus subtilis* sporulation. *eLife* **5**, e18657 (2016).
- 627 54. Chan, H. *et al.* Genetic Screens Identify Additional Genes Implicated in Envelope Remodeling during  
628 the Engulfment Stage of *Bacillus subtilis* Sporulation. *mBio* **13**, e01732-22 (2022).
- 629 55. Bravo, A., Agaisse, H., Salamitou, S. & Lereclus, D. Analysis of cryIAa expression in *sigE* and *sigK*  
630 mutants of *Bacillus thuringiensis*. *Mol Gen Genet* **250**, 734–741 (1996).
- 631 56. Peng, Q. *et al.* The Regulation of Exosporium-Related Genes in *Bacillus thuringiensis*. *Scientific*  
632 *Reports* **6**, 19005 (2016).
- 633 57. Manetsberger, J., Hall, E. A. H. & Christie, G. Plasmid-encoded genes influence exosporium assembly  
634 and morphology in *Bacillus megaterium* QM B1551 spores. *FEMS Microbiol Lett* **362**, fmv147 (2015).
- 635 58. McPherson, S. A., Li, M., Kearney, J. F. & Turnbough, C. L. ExsB, an unusually highly phosphorylated  
636 protein required for the stable attachment of the exosporium of *Bacillus anthracis*. *Molecular Microbiology*  
637 **76**, 1527–1538 (2010).
- 638 59. Todd, S. J., Moir, A. J. G., Johnson, M. J. & Moir, A. Genes of *Bacillus cereus* and *Bacillus anthracis*  
639 Encoding Proteins of the Exosporium. *Journal of Bacteriology* **185**, 3373–3378 (2003).
- 640 60. Kim, H. *et al.* The *Bacillus subtilis* spore coat protein interaction network. *Molecular Microbiology*  
641 **59**, 487–502 (2006).

- 642 61. Freitas, C. *et al.* A protein phosphorylation module patterns the *Bacillus subtilis* spore outer coat.  
643 *Molecular Microbiology* **114**, 934–951 (2020).
- 644 62. Saggese, A. *et al.* Antagonistic Role of CotG and CotH on Spore Germination and Coat Formation in  
645 *Bacillus subtilis*. *PLOS ONE* **9**, e104900 (2014).
- 646 63. Sacco, M., Ricca, E., Losick, R. & Cutting, S. An additional GerE-controlled gene encoding an  
647 abundant spore coat protein from *Bacillus subtilis*. *Journal of Bacteriology* **177**, 372–377 (1995).
- 648 64. Saggese, A. *et al.* CotG Mediates Spore Surface Permeability in *Bacillus subtilis*. *mBio* **0**, e02760-22  
649 (2022).
- 650 65. Haraldsen, J. D. & Sonenshein, A. L. Efficient sporulation in *Clostridium difficile* requires disruption  
651 of the  $\sigma^K$  gene. *Molecular Microbiology* **48**, 811–821 (2003).
- 652 66. Abe, K. *et al.* Regulated DNA rearrangement during sporulation in *Bacillus weihenstephanensis*  
653 KBAB4. *Molecular Microbiology* **90**, 415–427 (2013).
- 654 67. Klee, S. R. *et al.* The Genome of a *Bacillus* Isolate Causing Anthrax in Chimpanzees Combines  
655 Chromosomal Properties of *B. cereus* with *B. anthracis* Virulence Plasmids. *PLOS ONE* **5**, e10986 (2010).
- 656 68. Gustafsson, M. G. L. Surpassing the lateral resolution limit by a factor of two using structured  
657 illumination microscopy. *Journal of Microscopy* **198**, 82–87 (2000).
- 658 69. Heintzmann, R. Saturated patterned excitation microscopy with two-dimensional excitation  
659 patterns. *Micron* **34**, 283–291 (2003).
- 660 70. Betzig, E. Excitation strategies for optical lattice microscopy. *Opt. Express, OE* **13**, 3021–3036 (2005).
- 661 71. Delerue, T. *et al.* Bacterial developmental checkpoint that directly monitors cell surface  
662 morphogenesis. *Developmental Cell* **57**, 344–360.e6 (2022).
- 663 72. Costes, S. V. *et al.* Automatic and Quantitative Measurement of Protein-Protein Colocalization in  
664 Live Cells. *Biophysical Journal* **86**, 3993–4003 (2004).
- 665 73. Lereclus, D., Arantès, O., Chaufaux, J. & Lecadet, M.-M. Transformation and expression of a cloned  
666  $\delta$ -endotoxin gene in *Bacillus thuringiensis*. *FEMS Microbiology Letters* **60**, 211–217 (1989).
- 667 74. Sanchis, V., Agaisse, H., Chaufaux, J. & Lereclus, D. Construction of new insecticidal *Bacillus*  
668 *thuringiensis* recombinant strains by using the sporulation non-dependent expression system of cryIIIA and  
669 a site specific recombination vector. *Journal of Biotechnology* **48**, 81–96 (1996).

670

## 671 **Figure legends**

672 **Figure 1. Assembly of proteinaceous spore surface layers during *Bacillus cereus* sporulation.** Schematic  
673 illustration of *B. cereus* sporulation stages and transmission electron microscopy (TEM) image of a *B. cereus*  
674 ATCC 10876 spore. A tight control coordinates  $\sigma^K$  activation and engulfment completion across *Firmicutes*

675 species, but whether  $\sigma^K$  activation strictly depends on engulfment completion in *B. cereus* is unknown. Se-  
676 quence of coat (cyan) and exosporium (pink) formation as described by TEM in wild-type (WT) and  $\Delta cotE$   
677 strains<sup>15,18</sup>. Similar phenotypes were described in *B. anthracis*. In absence of exosporium cap in  $\Delta cotE$  mutant  
678 sporangia, coat deposition sequence is modified compared to that of the WT. MCD, Mother Cell Distal; MCP,  
679 Mother Cell Proximal pole of the forespore; FS, Forespore; MC, Mother Cell.

680 **Figure 2. TMR-star and MTG bind to the forespore surface after engulfment completion.** (A) WT14579  
681 or (B) congenic  $\Delta cotE$  cells sporulating at 20°C in SMB were labeled with TMR-star (TMR, red on merged  
682 images) and MTG (green on merged images) dyes and imaged with structured illumination microscopy (SIM)  
683 and bright field (BF) microscopy. Representative sporangia (panels *a-g*) or spores (panel *h*) observed at indi-  
684 cated times after resuspension in SMB medium are shown. Sporulation stages are indicated and stages writ-  
685 ten in red point the presence of TMR-star and MTG bright signals on the forespore surface. Yellow arrows  
686 bright MTG signals reflecting patterns of coat deposition according to previous TEM analysis in similar genetic  
687 backgrounds. Cyan arrows point to the TMR-star signal observed on the forespore surface. Yellow asterisks  
688 indicate refringent forespores and spores. Pink arrows point to the exosporium. Red boxes in MTG channel  
689 illustrate areas used to perform quantification of FS/MC MTG signal intensity ratio, as presented in Fig. 3.  
690 Scale bar in panel *a* represents 1  $\mu\text{m}$ .

691 **Figure 3. Quantification of MTG signal in sporangia at different sporulation stages.** (A) Boxplots show-  
692 ing quantification of MTG fluorescent signals ratio intensity between the forespore (FS) and the mother cell  
693 (MC) membranes in WT ATCC14579 (blue boxes),  $\Delta cotE$  (orange boxes) and in engulfment-defective (green  
694 boxes) sporangia in *B. cereus* ATCC 10876 sporulating at 20°C. The indicated sporulation stages refer to the  
695 Fig. 2A/B for WT14579 and  $\Delta cotE$ , respectively. For engulfment-defective sporangia, quantification was per-  
696 formed towards the MCP and the MCD regions. (B) Illustrations of the regions used for recording the MTG  
697 fluorescence intensity in representative engulfment-defective cells. Cells are from at least two independent  
698 experiments and fluorescence intensity was recorded in pseudo-widefield images (see Materials and meth-  
699 ods). Dashed red line represents a ratio of FS/MC MTG signal intensity=1. Each dot represents a different  
700 sporangia and n, the number of sporangia used for the quantification. The median values are indicated. The  
701 non-parametric Mann-Whitney U test was used, ns; not significant; \*\*,  $p < 0.005$ ; \*\*\*\*,  $p < 0.00005$ .

702 **Figure 4. Fluorescence SIM and TEM analysis reveal a coat bearding phenotype in engulfment-defec-**  
703 **tive *B. cereus* cells.** WT10876 cells sporulating at 20°C in SMB were imaged (A) with SIM and BF illumination  
704 modes after labeling with TMR-star and MTG or (B) by TEM after thin sectioning. (A) Typical sporangia show-  
705 ing an engulfment-defective phenotype detected at hour 24 and not presenting TMR-star or MTG bright  
706 signals (“bulging”, panels *a-c*) or at hour 48 and showing TMR-star and MTG signals (“bearding”, panels *d-e*)  
707 are shown. Sporangia with an engulfed refringent forespore detected at hour 48 (panel *g*) and spores to-  
708 gether with lysis fragments observed at hour 72 (panel *f*) are also shown for comparison. Cyan arrows indicate

709 TMR-star signal, yellow arrows show curved MTG bright signal and red arrows point to MTG bright signal  
710 drawing a straight line in the medial focal plan. Pink arrow points to the exosporium. Scale bar is 1  $\mu\text{m}$ . **(B)**  
711 WT10876 cells sporulating at 20°C, collected at hour 48 showing a blocked engulfment observed with TEM.  
712 Yellow arrow points to the large bearding coat fragment and red arrow points to the smaller fragments of  
713 coat disseminated in the MC cytoplasm. Pink arrow points at exosporium material. Right panel shows an inset  
714 of the junction between the FS (in green) and the MC (in magenta) compartments separated by peptidoglycan  
715 (PG) material (brown). Polymerized coat fragments (black dashed line) are present until the leading edge of  
716 the MC membranes. Scale bar represents 0.6  $\mu\text{m}$ .

717 **Figure 5. Detection of TMR-star signal on the forespore surface and specific BxpB-SNAP-TMR-star**  
718 **signal both depend on  $\sigma^K$ .** **(A-B)** WT407 or **(C-D)**  $\Delta sigK$  cells sporulating at 20°C and expressing the indicated  
719 SNAP fusion were collected at hour 24, labeled with TMR-star (red) and MTG (green) dyes and imaged by  
720 conventional fluorescence microscopy and phase contrast (PC) microscopy. **(E-G)** Sporangia of WT10876  
721 without SNAP fusion (“No fusion”), with BxpB-SNAP, and  $\Delta exsY$  with BxpB-SNAP were collected after hour 48  
722 and analyzed with conventional fluorescence microscopy and phase contrast (PC) microscopy after dual la-  
723 beling with TMR-star and MTG. Red asterisks indicate sporangia with an apparent “bearding” phenotype.  
724 Orange arrows indicate TMR-star signal observed in engulfment-defective sporangia. Cyan arrows point to  
725 TMR-star binding on the surface of refringent forespore (FS) surface. Pink arrows point at the specific signal  
726 from TMR-star binding on indicated SNAP-fusion. White arrows indicate linescan used to quantify TMR-star  
727 fluorescence intensity along the indicated cell; the intensity line profile are shown in B, D, F and G. Red box  
728 highlights TMR-star signal localized in the mother cell (MC) cytoplasm and the mean fraction of the fluores-  
729 cence intensity recorded in the FS is indicated (n = 25 cells; SD; standard deviation). A. U, Arbitrary Unit. ND,  
730 not determined. Scale bar in panel A represents 1  $\mu\text{m}$ . Merged images represent TMR-star and MTG channels  
731 superimposed. **(H)** Percentage of “bearding” sporangia detected at hour 48 in the indicated strain (See Ma-  
732 terials and Methods). Error bar represents SD of three biological replicates.

733 **Figure 6. BxpB-SNAP-TMR-star signal is specifically detected in sporangia showing a bearding pheno-**  
734 **type.** **(A-B)** Co-localization analysis for TMR-star and MTG signals in  $\Delta exsY$  spores, in exosporium cap or in  
735 bearding sporangia expressing the indicated SNAP fusion. Sporulation was performed in SMB at 20°C, col-  
736 lected at hour 72, labeled with TMR-Star and MTG dyes and imaged with lattice-SIM. **(A)** Representative co-  
737 localization maps generated by the co-localization threshold plugin on Fiji. Grey color indicates co-localiza-  
738 tion of MTG and TMR-star signals, green color indicates a preferential MTG signal enrichment and red color  
739 indicates predominant TMR-star signals. Scale bars represent 0.8  $\mu\text{m}$ . **(B)** Boxplots showing quantification of  
740 Pearson coefficient for TMR-star and MTG signals in  $\Delta exsY$  without fusion (blue boxes), with CotY-SNAP (or-  
741 ange boxes) or with BxpB-SNAP (green boxes). A dashed red line indicates a positive correlation ( $r > 0.5$ ).  
742 Median values are indicated. Each dot represents a different sporangia and n, the number of sporangia used

743 for quantification. The median values are indicated. (C) Z-projections of coat fragments released after lysis of  
744 bearding cells. TMR-star signals are in magenta and MTG signals represented in green. Scale bar represents  
745 0.8  $\mu\text{m}$ .

#### 746 **Table 1. Strains and plasmids used in this study**

747

#### 748 **Acknowledgments**

749 We thank Pr Mariana Pinho for providing access to the SIM PS1 microscope, Pedro Matos for very  
750 efficient training on image acquisition and analysis software and Dr Cécile Morlot for fruitful discussions. We  
751 also thank Dr Leyla Slamti for the gift of WT407 and  $\Delta sigK$  strains, Pr Anne Moir for  $\Delta exsY$  and  $\Delta cotY$  mutant  
752 strains and Dr Sandrine Poncet for pHT304-*pspoIIQ*-YFP plasmid.

753

#### 754 **Author contributions**

755 Conceptualization, A.L., V.B., A.O.H, F.C; methodology, A.L., S.C., C.B., M.S., I.B.; formal analysis, A.L., V.B.,  
756 visualization, A.L.; writing original draft, A.L.; writing, review and editing, A.L., V.B., A.O.H, F.C, RCL; project  
757 administration and funding acquisition, V.B., supervision, V.B., F.C. All authors have read and approved the  
758 final manuscript.

759

#### 760 **Funding**

761 The Ph.D. thesis of A.L. was funded by INRAE and the PACA Region and was partly supported by a grant of  
762 the MICA division and a Perdiguier grant of Avignon University. Part of this work was supported by the  
763 microscopy facilities of the Platform 3A, funded by the European Regional Development Fund, the French  
764 Ministry of Research, Higher Education and Innovation, the Provence-Alpes-Côte d'Azur region, the  
765 Departmental Council of Vaucluse and the Urban Community of Avignon. This work was also funded through  
766 grants PEst-OE/EQB/LA0004/2011 to AOH, by project LISBOA-01-0145-FEDER-007660 ("Microbiologia  
767 Molecular, Estrutural e Celular") funded by FEDER funds through COMPETE2020 – "Programa Operacional  
768 Competitividade e Internacionalização", and by project PPBI - Portuguese Platform of BioImaging (PPBI-POCI-  
769 01-0145-FEDER-022122) co-funded by national funds from OE - "Orçamento de Estado" and by European  
770 funds from FEDER - "Fundo Europeu de Desenvolvimento Regional". Work and Lattice SIM imaging in the  
771 R.C-L. lab was supported by funding from the European Research Council (ERC) under the Horizon 2020  
772 research and innovation program (grant agreement No 772178, ERC Consolidator grant to R.C.-L.).

773

#### 774 **Competing interests**

775 Authors declare no competing interests.

776

777 **Additional information**

778 Supplementary figures S1-S3



779 **Table 1.** Strains and plasmids used in this study

Strains or plasmids	Name	Relevant characteristic(s) or description	Source or reference
<i>Bacillus cereus</i>	ATCC 14579 wo	Wild type; cured from pClin15 plasmid	laboratory collection
	ATCC 14579 $\Delta cotE$	<i>cotE::spc</i>	47
	ATCC 10876	Wild type	26
	ATCC 10876 $\Delta exsY$	<i>exsY::spc</i>	20
<i>B. thuringiensis</i>	407 <i>cry-</i>	Wild type; acrysaliferous strain	73
	407 <i>cry-</i> $\Delta sigK$	$\Delta sigK::kan$ ; <i>sigK</i> (shares 100% AA sequence identity with ATCC 10876 and ATCC 14579 homologous sequences)	55
<i>E. coli</i>	DH5 $\alpha$	<i>fhuA2 lacU169 phoA glnV44 80= lacZM15 gyrA96 recA1 relA1 endA1 thi-1 hsdR17 L</i>	laboratory collection
	SCS110	<i>rpsL thr leu endA thi-1 lacY galK galT ara tonA tsx dam dcm supE44 (lac-proAB)</i>	laboratory collection
Plasmids	pHT304-18	Amp <sup>r</sup> Ery <sup>r</sup>	74
	pHT304-CotESNAP	Amp <sup>r</sup> Ery <sup>r</sup> ; BC3770 sequence of ATCC 14579 (shares 100% AA sequence identity with ATCC 10876 and WT407 homologous sequences)	15
	pHT304-CotYSNAP	Amp <sup>r</sup> Ery <sup>r</sup> ; BC1222 sequence of ATCC 14579 (shares 92.9% AA sequence identity with ATCC 10876 and WT407 homologous sequences)	15
	pHT304- <i>pspIIQ</i> -YFP	Amp <sup>r</sup> Ery <sup>r</sup> ; 355 bp upstream of <i>bthur0002_51550</i> sequence of WT407	Poncet <i>et al</i> , unpublished
	pHT304-BxpBSNAP	Amp <sup>r</sup> Ery <sup>r</sup> ; BC1221 sequence of ATCC 14579 (shares 98.2% AA sequence identity with ATCC 10876 and WT407 homologous sequences)	this study

780  
781  
782

Figure 1

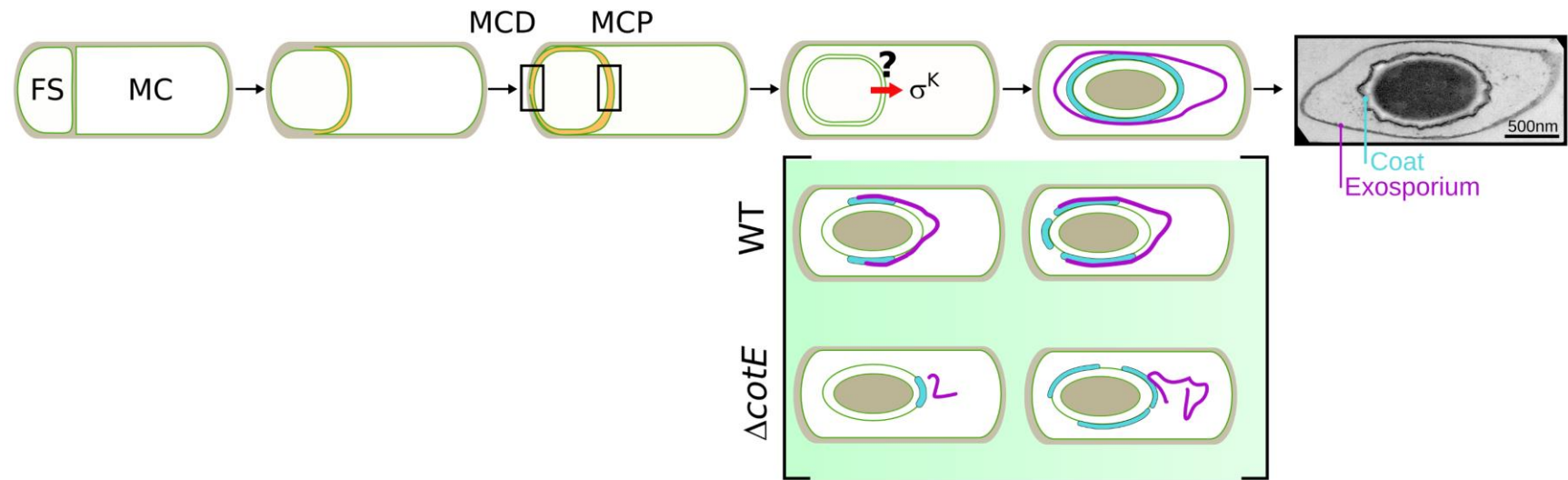


Figure 2

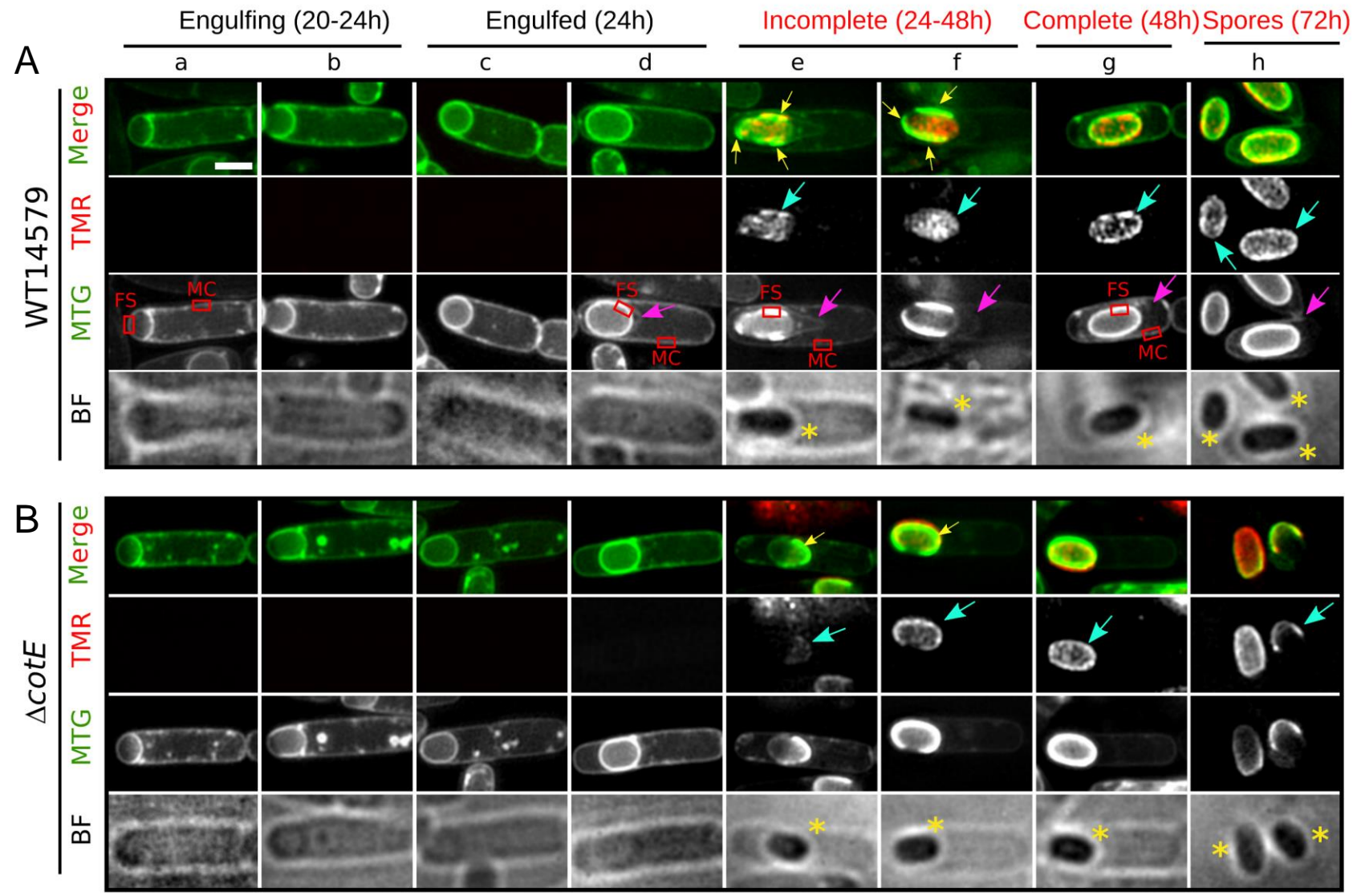


Figure 3

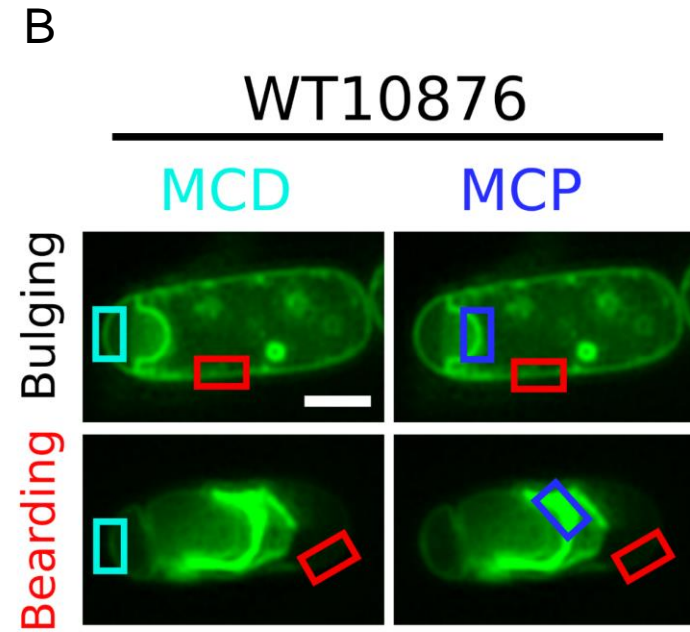
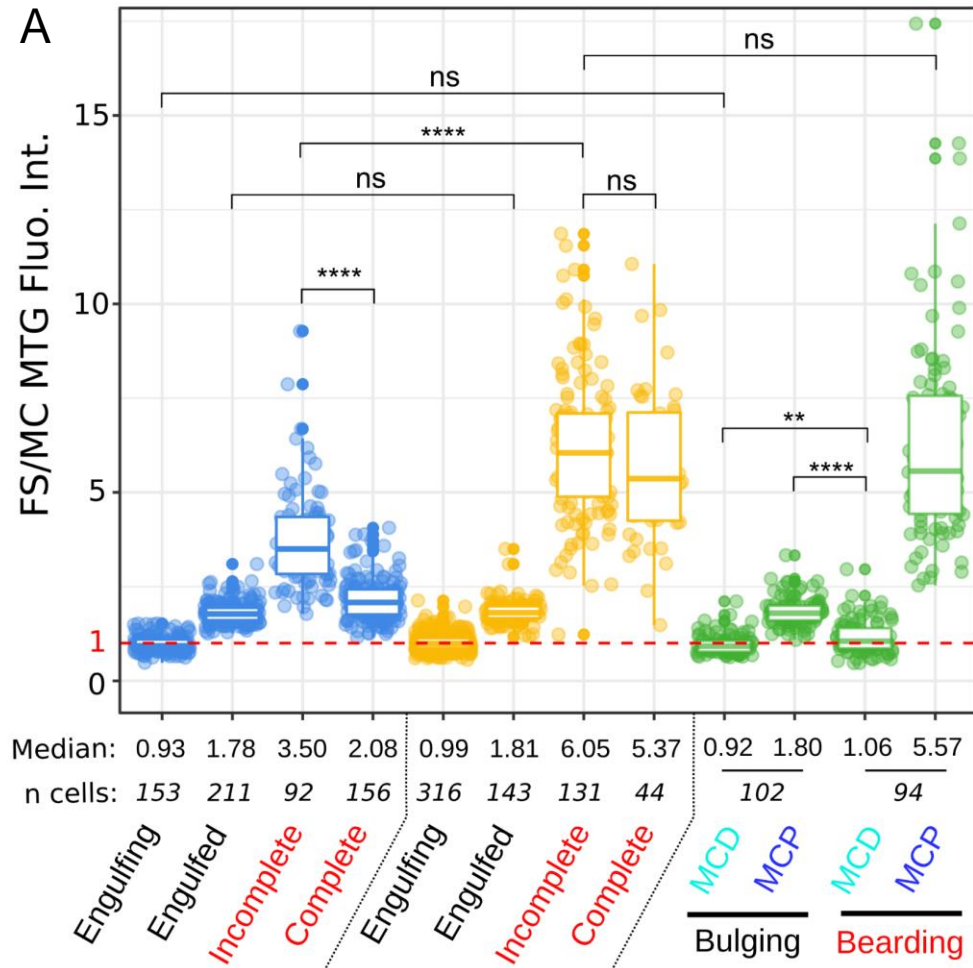


Figure 4

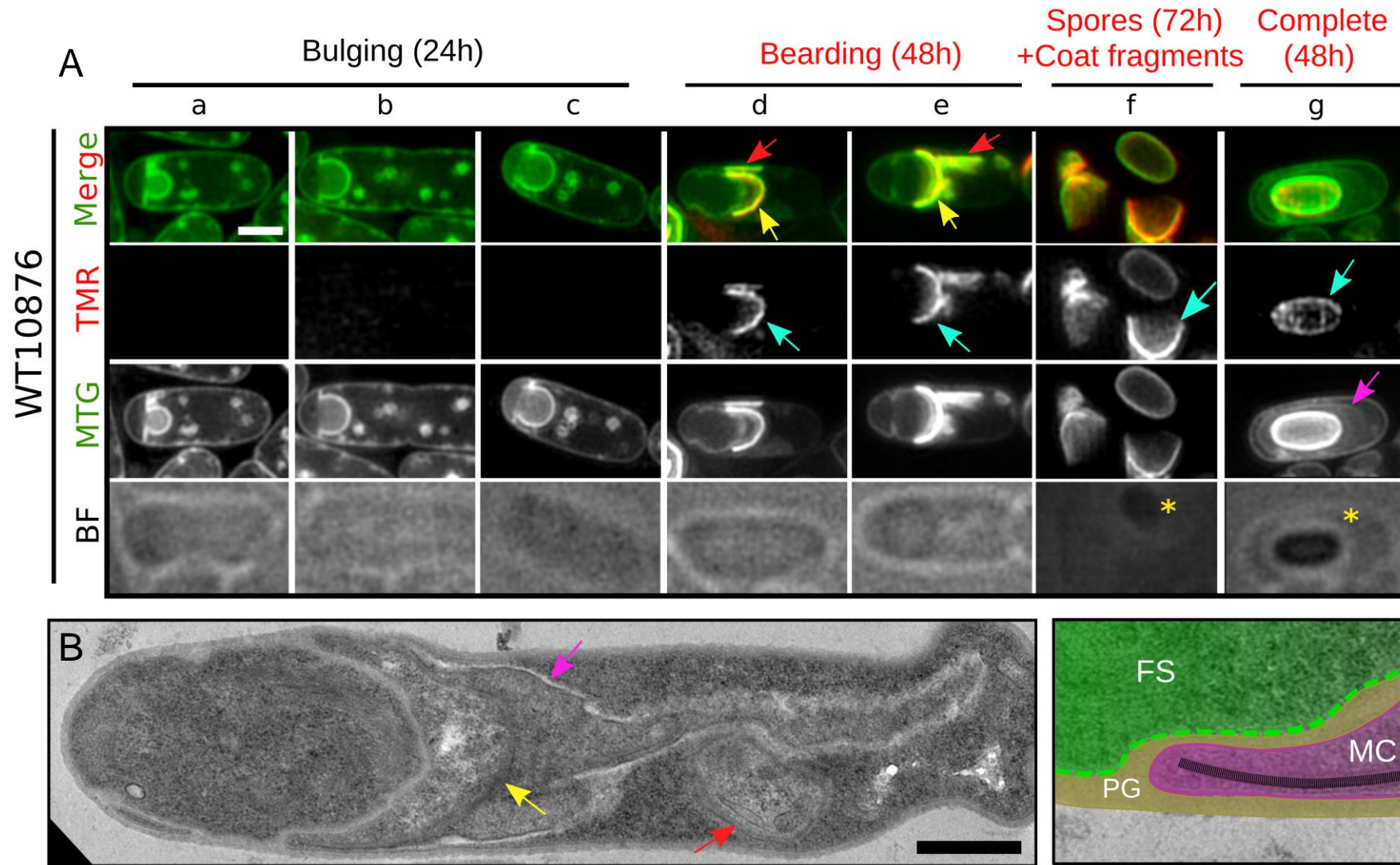


Figure 5

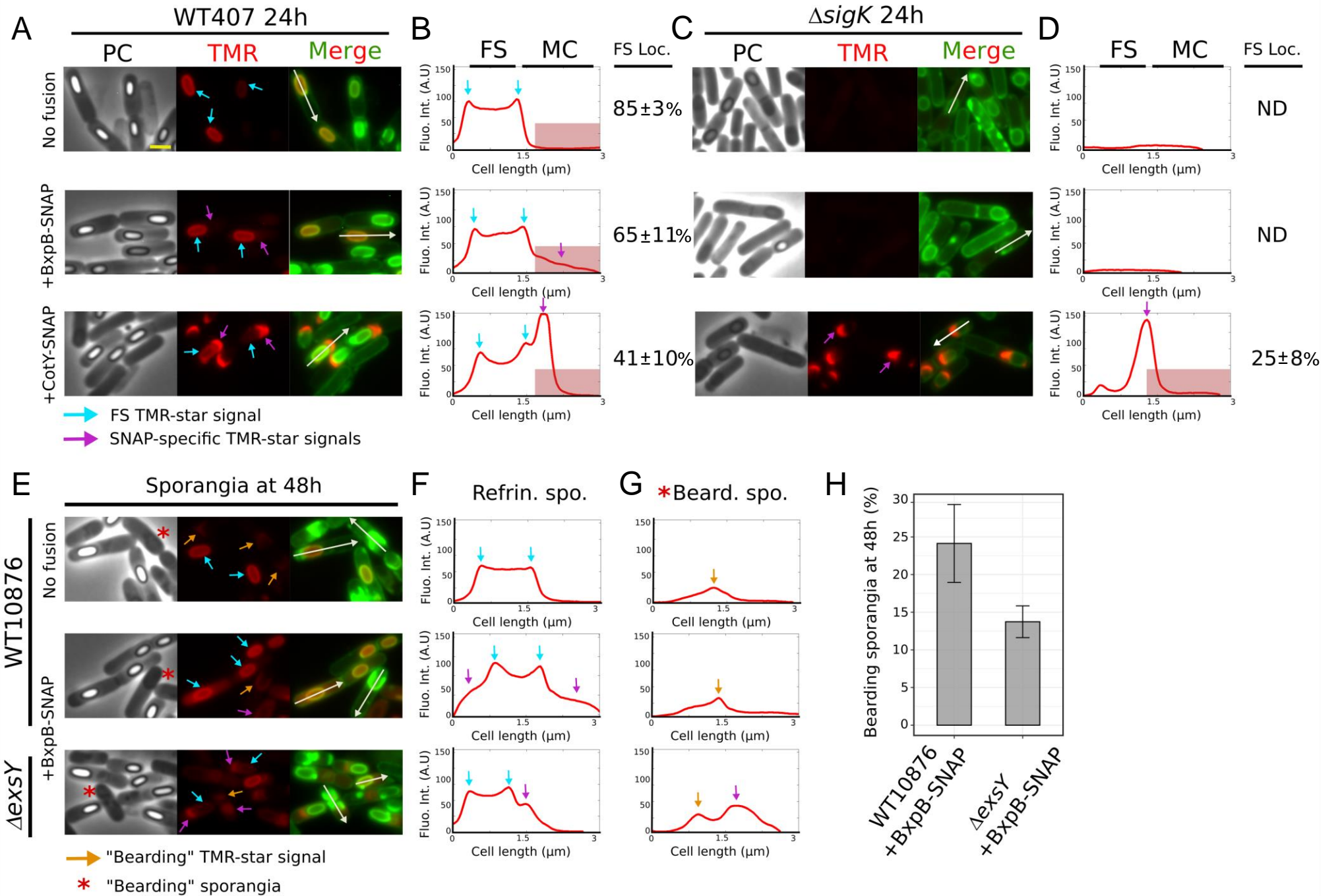


Figure 6

